Modeling the buckling and delamination of thin films

E. A. Jagla
Centro Atómico Bariloche, Comisión Nacional de Energía Atómica, (8400) Bariloche, Argentina
(Received 22 August 2006; revised manuscript received 30 November 2006; published 5 February 2007)

I study numerically the problem of delamination of a thin film elastically attached to a rigid substrate. A nominally flat elastic thin film is modeled using a two-dimensional triangular mesh. Both compression and bending rigidities are included to simulate compression and bending of the film. The film can buckle (i.e., abandon its flat configuration) when enough compressive strain is applied. The buckled configurations of a piece of film with stripe geometry are investigated as a function of the compressive strain. It is found that the stable configuration depends strongly on the applied strain and the Poisson ratio of the film. Next, the film is considered to be attached to a rigid substrate by springs that can break when the detaching force exceeds a threshold value, producing partial delamination of the film. Delamination is induced by a mismatch of the relaxed configurations of film and substrate. The morphology of the delaminated film can be followed and compared with available experimental results as a function of model parameters. "Telephone-cord," polygonal, and "brainlike" patterns qualitatively similar to experimentally observed configurations are obtained in different parameter regions. The main control parameters that select the different patterns are the strain mismatch between film and substrate and the degree of in-plane relaxation within the unbuckled regions.

DOI: 10.1103/PhysRevB.75.085405 PACS number(s): 68.55.−a, 68.35.−p

I. INTRODUCTION

The use of a variety of coatings to enhance the performance of materials is widespread in many areas of science and technology. The deposition of the coating usually occurs at conditions (such as temperature, humidity of the environment, etc.) very different from those to be found under work conditions. Due to this fact and to the different nature of substrate and coating, typically large mismatch stresses appear between the film and the substrate.[1] When the stresses are tensile on the film, this may fail due the nucleation of cracks that split the film to reduce to the total mechanical energy of the system. A familiar example of this phenomenon is the cracking observed sometimes in paints and in the surface of mud.[2] When mismatch stresses are compressive within the film, the most common mode of failure is called delamination:[1,3,4] the film partially detaches from the substrate to relieve the accumulated stress. Experimentally, different morphologies of the delaminated regions have been observed. In many cases delaminated regions of characteristic undulated geometries (referred to as "telephone cords") appear.

Delamination can be understood on the basis of the well-known phenomenon of buckling of elastic structures.[5] The first quantitative description of the buckling of a one-dimensional elastic rod goes back to Euler. Upon compression, an elastic rod can reach a state in which the straight configuration is no longer the minimum-energy configuration. At that point the rod acquires a nonstraight configuration; namely, it buckles. For two-dimensional elastic membranes the same kind of instability exists, but the problem becomes mathematically much more involved. The equilibrium equations of a membrane were obtained by Foppl and von Karman (FvK).[6] The FvK equations are two nonlinear, coupled differential equations for the separation of a given point with respect to the flat configuration and for the Airy potential for the in-plane displacement. The in-plane displacement can be reconstructed from auxiliary (linear) differential equations once the Airy potential is known.

Delamination of a film that is elastically attached to a rigid substrate involves the interplay of two main ingredients. For a given initial form of a delaminated region (in which the interaction with the substrate is assumed to be absent) the FvK equations determine the profile of the buckled configuration. The buckled film produces forces on the border that tend to detach the film further. In this way the film can continue its detaching by this mechanism, with the configuration of the buckled film adapting to the instantaneous form of the buckled region. Thus, in general, buckling and delamination of the film must be solved self-consistently, and this is possible only numerically.

A direct numerical solution of the FvK equations is rather difficult, because of its nonlinear nature. This is why some scientists have considered the simulation of a more-or-less realistic film, consisting of atoms interacting via interatomic forces. The problem with this approach is that in order to be able to model the bending of the film, a few layers of atoms are necessary, making the simulations rather inefficient and suffering from important spurious effects associated with the anisotropy of the numerical lattice.[7] Here, to simulate the film I use the following strategy, which to a large extent eliminates the previously mentioned drawbacks.[8] The film is modeled on a physical basis as a two-dimensional triangular lattice formed by springs that account for the compression and stretching behavior of the material. In addition, bending springs are introduced at the nodes of the triangular lattice to account for the bending rigidity of the film. The model can be shown to be elastically isotropic (in linear approximation), describing a material with Poisson ratio $\nu=1/3$. Additional bending springs are added to change the value of ν in a controlled manner, keeping the system isotropic. By referring to the sketch in Fig. 1(a), each node i of the triangular lattice contributes with an elastic energy H_i of the form

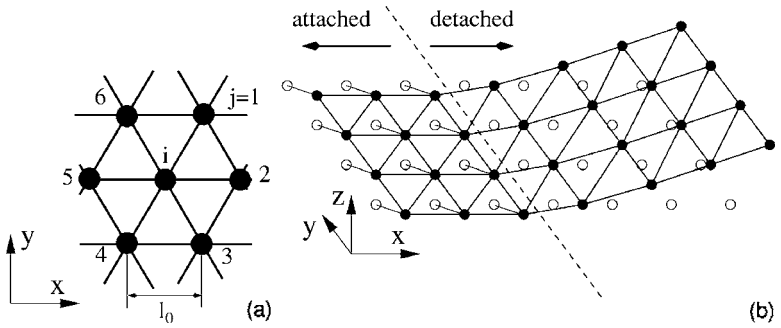

FIG. 1. (a) Detail of the triangular lattice that simulates the film, where the numbering of neighbors of site i and the equilibrium distance l_0 are highlighted. (b) A sketch of part of a partially delaminated film. Open symbols are the anchoring points in the substrate. The film is attached to the substrate to the left and is detached to the right. Note the possibility of horizontal relaxation in the attached part, indicated by the thin lines, along which the spring constant k_h is acting.

$$H_i = \sum_{j=1}^{6} \frac{1}{4} k_s [|\mathbf{u}_{ij}| - l_0]^2 + \sum_{j=1}^{3} k_b \left(\frac{\mathbf{u}_{ij} \cdot \mathbf{u}_{ij'}}{|\mathbf{u}_{ij}||\mathbf{u}_{ij'}|} + 1 \right) + \sum_{j=1}^{6} \frac{1}{2} k_\nu \left(\frac{\mathbf{u}_{ij} \cdot \mathbf{u}_{ij''}}{|\mathbf{u}_{ij}||\mathbf{u}_{ij''}|} - \frac{1}{2} \right)^2, \quad (1)$$

where $\mathbf{u}_{ij}$ is the vector joining sites i and j, the index j labels the six neighbors of site i, in sequential order, j' in the second term is $j+3$ (i.e., the neighbor opposite to neighbor j), and j'' in the last term is $j''=j+1$ for j from 1 to 5 and $j''=1$ for $j=6$. The three terms of this expression are, respectively, the stretching energy, the bending energy, and the corrective term that is introduced if a film with $\nu \neq 1/3$ is required. They are characterized by three different elastic constants: namely, k_s, k_b, and k_ν. The equilibrium configuration of a system described by the energy (1) is a flat triangular lattice with lattice parameter l_0.

From this atomistic expression for the energy of the system, the relation with averaged macroscopic quantities can be evaluated. The result for the bending rigidity D, the two-dimensional compressibility B, and the Poisson ratio ν of the bulk material of the film (which is assumed to have a thickness d) is[9]

$$B = \frac{\sqrt{3}}{d} k_s,$$

$$D = \frac{3\sqrt{3}}{4} k_b,$$

$$\nu = \frac{2l_0^2 k_s - 9k_\nu}{6l_0^2 k_s + 9k_\nu}. \quad (2)$$

The attaching (and eventual detaching) of the film to the substrate is the second crucial ingredient to be included in order to obtain a realistic behavior of the system. Experimentally, it has been emphasized that detaching by perpendicular separation has usually a much lower threshold than detaching by shear.[1] This suggests that an appropriate situation is to consider that detach occurs when the perpendicular force between film and substrate exceeds some maximum value f_{max}. This is implemented as follows. Let us consider the substrate to be located at $z=0$. For each node to be simulated in the film there is an anchoring point on the substrate to which this is attached to, prior to detaching. Let us suppose the coordinates of the anchoring point are $(x_0, y_0, 0)$ and those of the corresponding point in the film are (u_x, u_y, u_z). An elastic contribution to the energy of the form $\frac{1}{2}[k_h(u_x-x_0)^2+k_h(u_y-y_0)^2+k_z u_z^2]$ is then included. The vertical force between the node and its anchoring point is thus $k_z u_z$. If this force exceeds the maximum value f_{max} during the simulation, then the interaction of that node with the substrate is set irreversibly to zero, by putting $k_h=k_z=0$. The present scheme has been applied, for instance, in the simulations in Ref. 7, in the particular case of a stiff interaction with the substrate: namely, $k_h \to \infty$, $k_z \to \infty$ (in this limit the position of the node coincides with that of the anchoring point up to the rupture point). I have seen that this prescription does not suffice to reproduce the large phenomenology that is observed experimentally and think that the main lacking ingredient is the possibility of in-plane relaxation of the film in the case it is still attached to the substrate. Thus, I consider the possibility of finite values of k_h, which allow the film to relax horizontally, while it is still attached. The value of k_z is set to be infinitely large (additional simulations with a finite value of k_z indicate that this is not a very restrictive situation). Macroscopically, the attaching to the substrate can be quantified by an elastic coefficient I call E_s, which is defined as the ratio between the applied horizontal force per unit area of the film and the horizontal displacement this force produces. The relation between k_h and E_s is easily found to be

$$E_s = \frac{2k_h}{\sqrt{3}l_0^2}. \quad (3)$$

The anchoring points in the substrate form a triangular lattice, corresponding to that of the film. However, the lattice parameter of the anchoring-point lattice l_0^s is assumed to be smaller than the one l_0 in the film. This is the way in which a mismatch between film and substrate is introduced, and it is the origin of the tendency of the film to delaminate. The mismatch strain between film and substrate ε is defined as $\varepsilon \equiv (l_0/l_0^s - 1)$. All simulations presented below were made in systems with periodic boundary conditions in the x-y directions. To be more precise in the present case, the periodicity of the system is given by the lattice of anchoring points in the substrate, which has a lattice parameter l_0^s. The relaxed size of the film is a factor of l_0/l_0^s larger than this; this means that the film is compressed due to the boundary conditions, even if it is completely detached from the substrate.

In addition to the energetics, the time evolution of the system must be defined. This evolution will be assumed to be overdamped; namely, it is assumed that kinetic energy plays

no role in the evolution. Then the positions of the nodes of the lattice evolve according to

$$\frac{d\mathbf{u}}{dt} = -\lambda \frac{\delta H}{\delta \mathbf{u}}; \tag{4}$$

thus, λ sets the time scale for the evolution.

It is also convenient to introduce nondimensional parameters to describe the simulations. From Eqs. (1) and (4), it can be seen that the simulations can be parametrized by the values of $k_b/(l_0^2 k_s)$, $k_\nu/(l_0^2 k_s)$, k_h/k_s, and $f_{max}/(k_s l_0)$. A nondimensional time τ can also be introduced through $\tau=\lambda k_s t$. A first-order method was used to integrate Eq. (4), with a time step $\delta\tau=0.3$.

II. COMPARISON WITH ANALYTICAL RESULTS

As a validation test for the model, I will compare the results from simulations with available analytical results in simple geometrical configurations. Analytical results are available for a straight delaminated blister and a circular blister, and can be found in Ref. 10. In this section I take no horizontal relaxation in the nondelaminated regions (i.e., $k_h \to \infty$) since this is the condition applied in the calculations. The simplest configuration to study is the buckling of a stripe of material. When the stripe is loaded isotropically in compression (i.e., $\varepsilon>0$), the film remains flat until a critical value ε_1 is reached. At this point a uniform wrinkle along the longitudinal direction is formed. This configuration is usually referred to as the Euler column. The value of ε_1 can be analytically calculated, and it is known to be

$$\varepsilon_1 = \frac{4\pi^2 D}{w^2 B d}. \tag{5}$$

An equivalent expression can be obtained by expressing D and B in terms of the Young modulus of the material E, as indicated in Ref. 9. The result is

$$\varepsilon_1 = \frac{\pi^2 d^2}{3w^2(1+\nu)}, \tag{6}$$

where we see that the value of ε_1 is mainly controlled by the ratio between thickness and width of the delaminated stripe.

The value of ε_1 can also be expressed in terms of the parameters of the model by using Eqs. (2), as

$$\varepsilon_1 = \frac{4\pi^2}{(n+1)^2} \frac{k_b}{l_0^2 k_s}, \tag{7}$$

where n is the number of rows of nodes that compose the delaminated stripe [i.e., $w=\frac{\sqrt{3}}{2} l_0(n+1)$] and where the previously defined nondimensional parameter $k_b/(k_s l_0^2)$ appears.

In the Euler column configuration, the FvK equations become linear and can be solved analytically. The film takes a sinusoidal profile across the wrinkle for all values of the applied strain, and the amplitude of the buckled profile grows as $(\varepsilon/\varepsilon_1-1)^{1/2}$. In Fig. 2, I show some numerically obtained buckling profiles. They were obtained taking one of the main directions of the triangular simulation lattice along the stripe. The stripe was described by 24 rows of this triangular mesh, and the value of $k_b/(l_0^2 k_s)$ was taken to be 0.05 and $k_\nu=0$; i.e., a film with $\nu=1/3$ is being simulated. Due to the fact that we are seeking a homogeneous pattern along the stripe, only one lattice node (and periodic boundary conditions) was used in this direction. We can see that as long as the applied strain is small, the profile agrees very well with the analytical prediction, both in its form and in the buckling amplitude. The numerically obtained critical strain ε_1 coincides with the analytical value within an error of order $1/n$ where n is the number of rows that form the stripe. For very large values of the applied deformation, we see that the buckling profile departs from the sinusoidal form. This is actually not an artifact of the model, but instead a limitation of the FvK equations, for which the condition $\varepsilon \ll 1$ is assumed. From now on, in the rest of the paper I will restrict this study to cases in which ε does not reach these very large values. In this case, the strain enters into the problem only in the combination $\varepsilon/\varepsilon_1$.

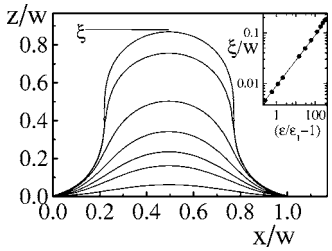

FIG. 2. Homogeneous buckling profiles of a stripe for different values of $\varepsilon/\varepsilon_1$, obtained in simulations with $n=24$ and $k_b/l_0^2 k_s=0.05$. Inset: measured buckling amplitudes as a function of $\varepsilon/\varepsilon_1$. Dots are the simulated values, and the line is the analytical result. The critical strain ε_1 for the parameters used is $\varepsilon_1 \simeq 0.00315$.

Other interesting quantities to calculate in delamination problems are the energy release rate and the loading ratio at the edge of the delaminated blister. They are precisely defined in Ref. 10 and are analytically known for the Euler column. In the numerical implementation they are computed by calculating the in-plane compressive force and the bending moment per unit length at the border between delaminated and nondelaminated regions. In the top of Fig. 3 I plot the analytical values and the results from the simulations for the Euler column. We can see that the agreement is quite satisfactory.

A second configuration in which the FvK equations have been solved in detail is the circular blister. In this case the nonlinear nature of the FvK equations enters into play. Numerically obtained buckling profiles for the circular blister are shown in Fig. 4. Very close to the buckling threshold, the profile is analytically known to be given in terms of the J_0 Bessel function. In practice, this profile is hardly distinguishable from a sinusoidal profile. The change of the profile for larger values of $\varepsilon/\varepsilon_1$ (but still $\varepsilon \ll 1$) is a consequence of the nonlinear nature of the problem. The numerically obtained energy release rate and edge loading ratio, shown in the bottom of Fig. 3, agree very well with the forms given in Ref. 10.

III. BUCKLING PATTERNS OF A STRIPE

Now I consider the stability of the Euler column configuration when applied deformation increases. This case has

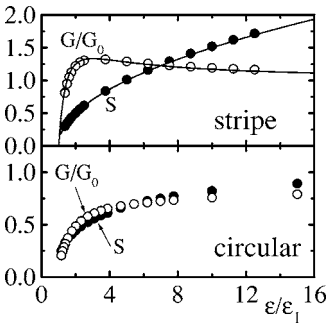

FIG. 3. Energy release rate G normalized by its analytical asymptotic value G_0 and edge loading ratio S at the edge of a stripe blister and a circular blister ($S=h\Delta N/\sqrt{12}M$ in the notation of Ref. 10). For the stripe geometry the solid lines are the exact results from Ref. 10. The results for the circular blister can be compared with those in Fig. 64 of Ref. 10.

been considered previously in the literature,[11] and then it will be useful to validate the numerical model. In addition we will see that already in this simple case the behavior is nontrivial. Thus we consider a stripe piece of the film of width w, which is detached from the substrate. The rest of the film is assumed to be rigidly attached to the substrate (i.e., $k_h \to \infty$). In this way, the only effect of this part of the film is to provide a clamped boundary condition for the stripe. In addition, due to the presence of the substrate, the stripe can buckle only toward positive values of z. Under these conditions we will look for a stable configuration of the stripe for different parameters.

The Euler column configuration mostly relieves the perpendicular stress on the stripe, but leaves an important degree of longitudinal compression in it. If the isotropic compression ε is increased, a secondary buckling is expected at some mismatch strain ε_2, in which the longitudinal uniformity of the Euler column is lost and one of two different patterns is expected:[11] in one case (occurring if the Poisson ratio ν of the film is larger than a value of approximately 0.255) the Euler column transforms into an undulated wrinkle. The second case corresponds to a pattern (sometimes called "varicose") appearing if ν is lower than this value, in which the uniform maximum of the Euler column is distorted and transforms into a sequence of small hills and shallow valleys. The varicose pattern preserves the symmetry of the configuration with respect to the axis of the delaminated region, whereas the undulated wrinkle does not. These results have been obtained analytically doing a perturbative analysis of the FvK equations considering small distortions of the Euler column. The analysis shows also[11] that $\varepsilon_2/\varepsilon_1$ is a function of the Poisson ratio of the film only. Using the numerical model presented here, we can test this prediction, and in addition we can explore arbitrary distortions of the film.

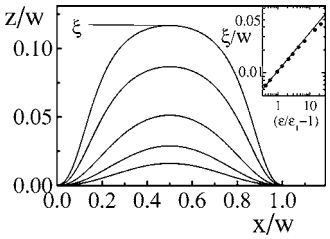

FIG. 4. Buckling profiles of the circular blister for different values of $\varepsilon/\varepsilon_1$ (a blister of radius $20l_0$ was used in the simulations). Inset: Measured buckling amplitude as a function of $\varepsilon/\varepsilon_1$. Dots are the simulated results, and the solild line is the asymptotic analytical behavior for $\varepsilon \to \varepsilon_1$. Critical strain ε_1 in this case is $\varepsilon_1 \simeq 0.00129$.

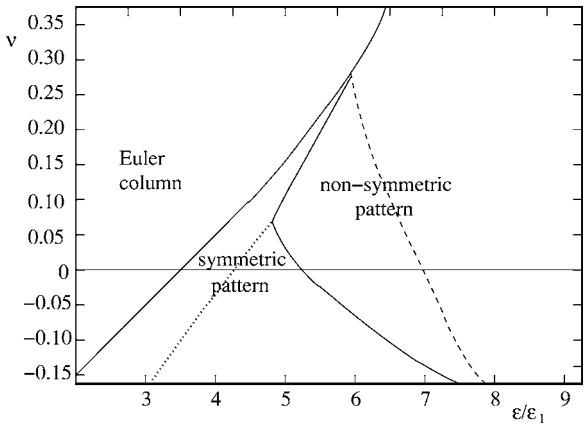

FIG. 5. The ν-ε parameter space, with the different sectors in which different qualitative behavior is observed. The lines separating different regimes were obtained by doing independent simulation at different points of the ε-ν plane. Some of them are presented in the next three figures. See the text and Figs. 6–8. Simulations were performed using a triangular lattice of 200 sites along the stripe and 24 rows in the perpendicular direction. The dimensionless combination of parameters $k_b/(k_s l_0^2)$ was taken to be 0.05.

Numerical results in the stripe geometry were obtained using the same parameters as those of the previous section, except that I take 200 nodes in the direction along the stripe to allow the appearance of nonhomogeneous patterns in that direction. Results are synthesized in the phase diagram of Fig. 5 and in Figs. 6–8, where the obtained configurations are shown for different values of the two main control parameters $\varepsilon/\varepsilon_1$ and ν. In agreement with the analytical predictions, we can see that by increasing ε, the instability of

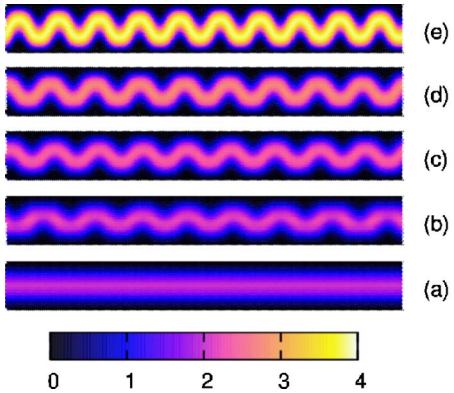

FIG. 6. (Color online) The buckled configuration of the stripe, for $\nu=1/3$ and $\varepsilon/\varepsilon_1=6.25$, 7.5, 9.4, 12.5, and 25, respectively, from (a) to (e). The gray (color) scale indicates the departure of the film from the substrate, in units of the discretization distance l_0 (in units of l_0 the width of the stripe is $25\sqrt{3}l_0/2$).

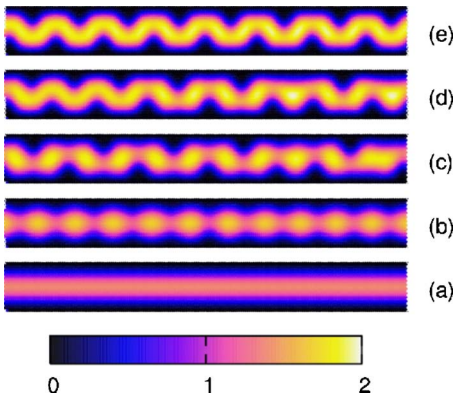

FIG. 7. (Color online) Same as Fig. 6 for $\nu=0.075$ and $\varepsilon/\varepsilon_1=4.0$, 4.7, 5.6, 6.25, and 6.9, respectively, from (a) to (e).

the Euler column corresponds to a nonsymmetric pattern for $\nu>\nu_c\simeq 0.25$, whereas it corresponds to a symmetric one for $\nu<\nu_c$. However, we also see that when larger values of ε are considered, the stability range of the symmetric pattern is (at least for $\nu\gtrsim 0.05$) only a rather small wedge in the phase diagram. For sufficiently large values of ε the undulated wrinkle pattern is observed always to be the stable one.

The symmetric and nonsymmetric sectors of the phase diagram in Fig. 5 have been divided by a dotted and dashed line, respectively. I describe now their meaning. The dashed line in the nonsymmetric sector marks only a crossover: At the right of this line, the undulated wrinkle is well developed, in the sense that it has a maximum of almost constant amplitude that undulates along the stripe; see, for instance, Fig. 7(e). At the left of the dashed line, there is a clear modulation of the amplitude [Fig. 7(c)]. I emphasize again that the transition between the two different behaviors is simply a crossover.

The dotted line within the symmetric sector in Fig. 5 marks an interesting behavior change in the region of small or negative values of ν. To the left of the dotted line we have the symmetric pattern as described analytically in Ref. 11. To the right of the dashed line, this pattern gets modified by the appearance of deep valleys interrupting the normal sequence of small hills and shallow valleys [see Fig. 8(c)]. Note that in the center of the deep valleys, the film is almost touching the substrate. The appearance of these deep valleys is abrupt;

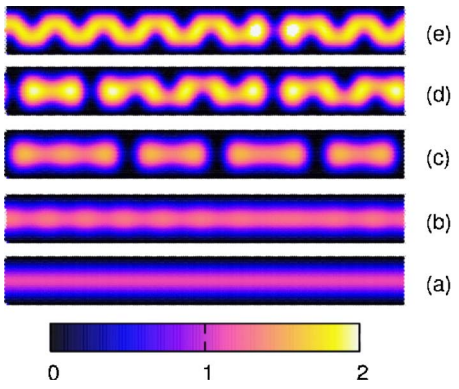

FIG. 8. (Color online) Same as Fig. 6 for $\nu=0$ and $\varepsilon/\varepsilon_1=3.12$, 3.75, 4.37, 6.25, and 6.9, respectively, from (a) to (e).

namely, they do not grow deeper and deeper as some parameter is changed, but they simply exist or do not exist. The periodicity of the appearance of deep valleys is difficult to obtain from the simulations, but the information collected from different simulations suggests that close to the dotted line of the phase diagram deep valleys are well separated from each other, whereas when moving to larger values of ε they become closer, eventually leaving no shallow valleys in between. A qualitative explanation for the appearance of these deep valleys could be based on the following observation. In a material with negative Poisson ratio, a compression in one direction is accompanied by a compression in the perpendicular direction. Transforming a shallow valley of a varicose pattern into a deep valley produces a compression in the direction perpendicular to the stripe, which implies a tendency to compress also in the direction along the stripe. In this way part of the longitudinal compression is relieved, and this can stabilize the deep valley. The observation of patterns with deep valleys for sufficiently low Poisson ratio seems to be correlated with the existence of a snapthrough transition occurring in the Euler column configuration of a film with $\nu\simeq 1/3$ under nonisotropic conditions, when compression along the stripe is increased.[12]

On the whole, the previous results show that, for the usual cases of materials with Poisson ratio close to 1/3, the undulated wrinkle pattern is the most likely to be observable in experimental situations in which stripe-delaminated regions occur.

IV. DELAMINATION

In this section I consider the full interplay of buckling and delamination, and present the different kinds of delamination morphologies that can be obtained with the present model. From now on I restrict the discussion to the case of a film with $\nu=1/3$ (i.e., $k_\nu=0$). When buckling and delamination both occur, there are two natural length parameters in the problem whose meaning is convenient to emphasize from the beginning. The first length scale L_1 is the typical size of a blister that is in equilibrium upon further delamination. An estimation of L_1 goes as follows. For a buckled region of typical linear size L_1 (L_1 may be, for instance, the diameter of a circular blister or the width of an Euler column) under a deformation ε, the typical curvature of the buckled film at the points of contact with the substrate is $\sim\sqrt{\varepsilon}/L_1$.[13] The torque T per unit length exerted by the delaminated film on the part attached to the substrate is obtained by multiplying this curvature by the bending rigidity D—i.e., $T\sim\sqrt{\varepsilon}D/L_1$. The equilibrium condition for the film will correspond to this torque been equal to a critical maximum value that the interaction with the substrate can sustain. I denote this maximum torque as T_{max}. Thus we obtain the order of magnitude of L_1 as $L_1\sim\sqrt{\varepsilon}D/T_{max}$. It is important to emphasize that the condition of a maximum torque per unit length that I use here is totally compatible with the condition of a maximum force used to describe the model in the previous section. In fact, note first of all that a torque per unit length has the correct units of a force. In addition, a detailed consideration of the geometry of the triangular lattice used shows that T_{max} in the

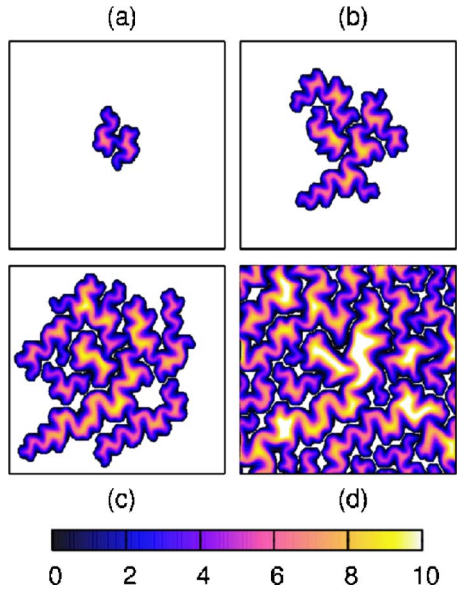

FIG. 9. (Color online) Temporal evolution of the delaminated regions for $\varepsilon=0.09$, $k_b/(k_s l_0^2)=0.05$, $f_{max}/(k_s l_0)=0.03$, and $k_h=k_s$. Note that the gray (color) scale goes from darker to brighter when the vertical coordinate of the film increases, but nondelaminated regions are plotted as white for clarity. Vertical scale is in units of l_0. Dimensionless time τ for the four views is $\tau=5\times10^3$, 2×10^4, 3.5×10^4, and 2×10^5.

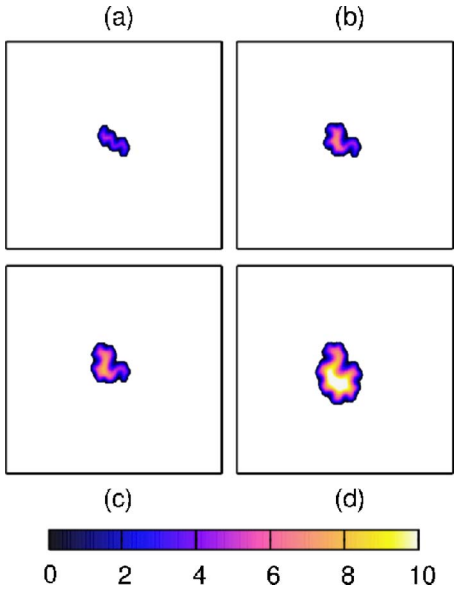

FIG. 10. (Color online) Same as Fig. 9 for $\varepsilon=0.085$ and $k_h=k_s$ at times $\tau=5\times10^3$, 2×10^4, 3.5×10^4, and 2×10^5. Note in particular that the last panel shows a stable configuration in which the film does not delaminate further.

continuum description and f_{max} of the atomistic description are simply related by $T_{max}=f_{max}\sqrt{3}/2$. Then, in the microscopic units of the model L_1 can be written also as $L_1 \sim \sqrt{\varepsilon k_b/f_{max}}$.

A second characteristic distance is related to the existence of horizontal relaxation within the unbuckled film. In fact, consider a film uniformly attached to the substrate. If we force a horizontal displacement of some point of the film, this perturbation will decay away in a typical distance L_2, which depends on the ratio between the stiffness of the film and the strength of the interaction to the substrate; namely, $L_2 \sim l_0\sqrt{k_s/k_h}$ or, in macroscopic units, $L_2 \sim \sqrt{Bd/E_s}$. The ratio L_2/L_1 is a measure of the importance of horizontal relaxation. This will be negligible if $L_2/L_1 \ll 1$ or important if $L_2/L_1 \gtrsim 1$.

In order to observe the delamination process, I seed the simulation with a configuration in which a small part of the film is detached. This portion was chosen as a small rectangular piece, misoriented with respect to the numerical mesh to minimize spurious effects associated with it. In a first stage of the simulation I take $f_{max}\to\infty$. In this way buckling of the seeded delaminated region occurs, but the film does not delaminate further. After a stationary configuration is achieved, f_{max} is put to a finite value, time is reset to zero, and the evolution of the film is calculated. In all cases presented the numerical lattice has a total of 300×300 nodes, and periodic boundary conditions are used.

I present first some result in the case in which horizontal relaxation is small: namely, $k_h=k_s$. This corresponds to a distance L_2 of the order of the discretization distance l_0—i.e., a very small value. In Fig. 9 we see a sequence of configurations corresponding to $\varepsilon=0.09$. We see how in this case the film delaminates almost completely. This kind of pattern was called "brain like" in Ref. 4. In Fig. 10 we see the situation for a slightly lower value of ε: namely, $\varepsilon=0.085$. After the delamination of a small region near the original defect, the evolution stopped completely and delamination halted. We see that there is a rather sharp transition between a blister that is not able to grow for low strains to an almost completely delaminated film for larger strains.

In the case in which the value of horizontal relaxation is higher, there are important differences in morphology. Figures 11, 12, and 13 show the evolution of the same original defect for the case of $k_h=k_s/100$ (which corresponds to a

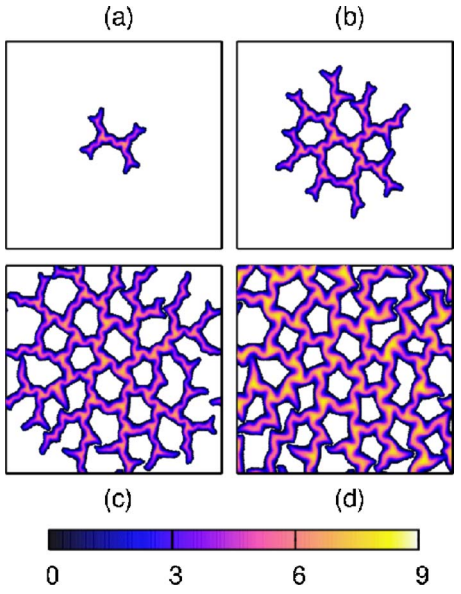

FIG. 11. (Color online) Same as Fig. 9 for $\varepsilon=0.09$ and $k_h=k_s/100$ at times $\tau=1.2\times10^3$, 3×10^3, 5.4×10^3, and 1.8×10^4.

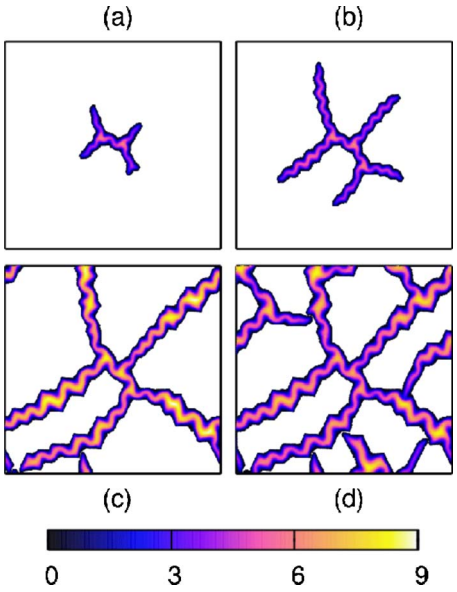

FIG. 12. (Color online) Same as Fig. 9 for $\varepsilon=0.07$ and $k_h=k_s/100$ at times $\tau=2.4\times10^3$, 5.4×10^3, 3.5×10^4, and 1×10^5.

relaxation distance L_2 approximately 10 times l_0) and $\varepsilon=0.09$, 0.07, and 0.065, respectively. For large values of the strain (Fig. 11), the delaminated region propagates to all the film; however, contrary to the previous case, there are large sectors in which the film remains attached to the substrate. The typical size of these sectors is roughly determined by L_2, whereas the typical width of the delaminated stripes between sectors is of order L_1. Note that the propagation occurs via

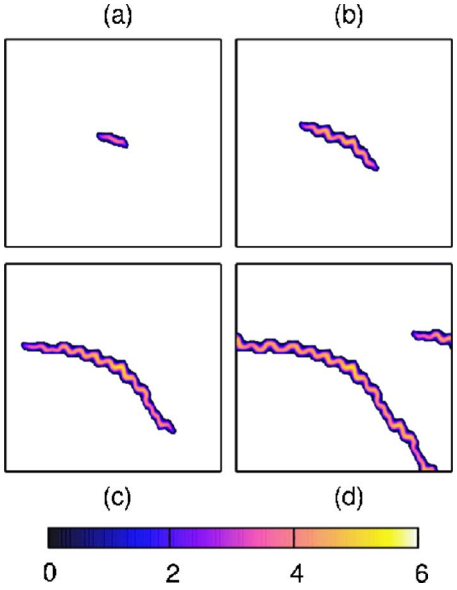

FIG. 13. (Color online) Same as Fig. 9 for $\varepsilon=0.065$ and $k_h=k_s/100$ at times $\tau=6\times10^2$, 3.6×10^3, 8.4×10^3, and 1.4×10^4. The curvature observed is due to a residual effect of the triangular lattice that defines the model.

the formation and branching of undulated blisters, which at the end form a pattern of polygons bounded by undulated wrinkles. When ε is reduced, the branching of the undulated blisters reduces, giving rise to a pattern like that in Fig. 12. In a narrow band of values of the applied strain (Fig. 13), branching does not occur and a "telephone cord" may be formed. For lower values of ε (not shown) the original blister is not able to grow at all.

V. CONCLUSIONS

I have presented results about the buckling of a thin film attached to a substrate. Buckling is induced by a mismatch in the relaxed configurations of film and substrate. For a fixed geometry of the delaminated region—namely, a uniform stripe—the buckling patterns were obtained as a function of the strain mismatch ε and the Poisson ratio of the film ν. The numerical results confirm the findings of previous analytic treatments about the instability mode of the uniform Euler column: a undulated wrinkle for $\nu\gtrsim0.25$ and a symmetric, "varicose" pattern for $\nu\lesssim0.25$. However, the present numerical analysis, which is not restricted to small distortions of the Euler column, shows that the stability of the varicose pattern, in the region of experimental interest close to $\nu\simeq1/3$, is restricted to a narrow interval of ε values, then limiting the possibility of observing this pattern experimentally.

In the second part of the paper I considered the interplay of buckling and delamination, and argued that a key factor determining the morphology observed is the possibility of horizontal relaxation in the nondelaminated part of the film. For small horizontal relaxation and large enough ε, the film delaminates almost completely, generating a "brainlike" structure. When ε is reduced, there is an abrupt transition to a situation in which the delaminated region is not able to grow.

For the case of large horizontal relaxation in the nondelaminated part of the film, at large ε the growing occurs via elongation and branching of undulated delaminated regions. At the end a polygonal pattern delimited by undulated stripes is observed. The main characteristic of this pattern is the existence of regions in which the film does not delaminate. When ε is reduced, the tendency of the undulated stripes to branch is reduced, and eventually a regime where a single undulated stripe (a "telephone cord") grows is observed. If ε is reduced further, the delamination stops completely.

The simulations presented clarify the origin of the different morphologies observed experimentally. I want to emphasize in particular the importance of horizontal relaxation in obtaining different kinds of patterns, most remarkably the necessity of horizontal relaxation to obtain the well-known telephone-cord pattern.

ACKNOWLEDGMENTS

This work was financially supported by Consejo Nacional de Investigaciones Científicas y Técnicas (CONICET), Argentina, under Grant No. PIP/5596.

[1] G. Gioia and M. Ortiz, Adv. Appl. Mech. **33**, 119 (1997).
[2] K. Leung and J. V. Andersen, Europhys. Lett. **38**, 589 (1997); S. Kitsunezaki, Phys. Rev. E **60**, 6449 (1999); A. Groisman and E. Kaplan, Europhys. Lett. **25**, 415 (1994); P. Meakin, Science **252**, 226 (1991); W. Korneta, S. K. Mendiratta, and J. Menteiro, Phys. Rev. E **57**, 3142 (1998); K. A. Shorlin, J. R. de Bruyn, M. Graham, and S. W. Morris, *ibid.* **61**, 6950 (2000); T. Hornig, I. M. Sokolov, and A. Blumen, *ibid.* **54**, 4293 (1996); K. T. Leung and Z. Neda, Phys. Rev. Lett. **85**, 662 (2000).
[3] J. Colin, F. Cleymand, C. Coupeau, and J. Grilhé, Philos. Mag. A **80**, 2559 (2000); F. Cleymand, C. Coupeau, and J. Grilhé, Scr. Mater. **44**, 2623 (2001); M.-W. Moon, H. M. Jensen, J. W. Hutchinson, K. H. Oh, and A. G. Evans, J. Mech. Phys. Solids **50**, 2355 (2002); M.-W. Moon, K.-R. Lee, K. H. Oh, and J. W. Hutchinson, Acta Mater. **52**, 3151 (2004).
[4] C. Coupeau, Thin Solid Films **406**, 190 (2002).
[5] S. P. Timoshenko and J. Gere, *Theory of Elastic Stability* (McGraw-Hill, New York, 1961).
[6] L. D. Landau and E. M. Lifshitz, *Theory of Elasticity* (Pergamon Press, Oxford, 1970).
[7] K. M. Crosby and R. M. Bradley, Phys. Rev. E **59**, R2542 (1999).
[8] This kind of strategy has been used in other contexts—for instance, to simulate the crumpling of an elastic membrane. See, for instance, J. A. Astrom, J. Timonen, and M. Karttunen, Phys. Rev. Lett. **93**, 244301 (2004), and references therein.
[9] To avoid confusion, note that D is related with the bulk Young modulus E of the material of the film by $D=\frac{Ed^3}{12(1-\nu^2)}$, and B (which is the proportionality between a given applied stress σ in the plane of the film and the corresponding strain ε: namely, $\sigma=B\varepsilon$) can be written also as $B=E/(1-\nu)$.
[10] J. W. Hutchinson and Z. Suo, Adv. Appl. Mech. **29**, 64 (1991).
[11] B. Audoly, Phys. Rev. Lett. **83**, 4124 (1999).
[12] G. Parry, J. Colin, C. Coupeau, F. Foucher, A. Cimetiere, and J. Grilhé, Appl. Phys. Lett. **86**, 081905 (2005).
[13] This estimation of the curvature is valid in the case when the applied ε is much larger than the corresponding ε_1 calculated for a blister of typical size L_1. This condition is typically satisfied in most experimental realizations.